

---

# Compressed Predictive Information Coding

---

Rui Meng<sup>1</sup> Tianyi Luo<sup>2</sup> Kristofer Bouchard<sup>1</sup>

## Abstract

Unsupervised learning plays an important role in many fields, such as artificial intelligence, machine learning, and neuroscience. Compared to static data, methods for extracting low-dimensional structure for dynamic data are lagging. We developed a novel information-theoretic framework, Compressed Predictive Information Coding (CPIC), to extract useful representations from dynamic data. CPIC selectively projects the past (input) into a linear subspace that is predictive about the compressed data projected from the future (output). The key insight of our framework is to learn representations by minimizing the compression complexity and maximizing the predictive information in latent space. We derive variational bounds of the CPIC loss which induces the latent space to capture information that is maximally predictive. Our variational bounds are tractable by leveraging bounds of mutual information. We find that introducing stochasticity in the encoder robustly contributes to better representation. Furthermore, variational approaches perform better in mutual information estimation compared with estimates under a Gaussian assumption. We demonstrate that CPIC is able to recover the latent space of noisy dynamical systems with low signal-to-noise ratios, and extracts features predictive of exogenous variables in neuroscience data.

## 1. Introduction

Unsupervised methods play an important role in learning robust representations that provide insight into data and exploit unlabeled data to improve performance in downstream tasks in diverse application areas (Bengio et al., 2013; Chen et al., 2020; Grill et al., 2020; Devlin et al., 2018; Brown et al., 2020; Baeviski et al., 2020; Wang et al., 2020). Prior

work on unsupervised representation learning can be broadly categorized into generative models such as variational autoencoders (VAEs) (Kingma & Welling, 2013) and generative adversarial networks (GAN) (Goodfellow et al., 2014), and contrastive models such as contrastive predictive coding (CPC) (Oord et al., 2018) and deep autoencoding predictive components (DAPC) (Bai et al., 2020). Generative models focus on capturing the joint distribution between representations and inputs, but are usually computationally expensive. On the other hand, contrastive models emphasize capturing the similarity structure of data in the low-dimensional representation space, and are therefore easier to scale to large datasets.

In the case of sequential (i.e., dynamic) data, some representation learning models take advantage of an estimate of mutual information between encoded input past and output future (Creutzig & Sprekeler, 2008; Creutzig et al., 2009; Oord et al., 2018). Although those models provide useful representations, they are nonetheless sensitive to noise in the observational space. Dynamical Components Analysis (DCA) (Clark et al., 2019) directly makes use of the mutual information between the past and the future (i.e., the predictive information (Bialek et al., 2001)) in the latent representational space. (Bai et al., 2020) extend DCA to make use of nonlinear representations by leveraging neural networks.

We focus on the problem of learning compressed representations of sequential data for downstream prediction tasks. A popular approach in the unsupervised representation learning literature is to use deep encoder networks to model nonlinear relations between representations and inputs (Chen et al., 2020; Bai et al., 2020; He et al., 2020). However, use of nonlinear encoders makes interpretation of the learned features difficult. Therefore, we choose to employ a linear encoder (i.e., identify optimal linear subspaces) as in (Clark et al., 2019; Wang et al., 2019). We evaluate the quality of the representation by measuring how well the model can capture the true generative dynamics in synthetic experiment, and how well the model performs on forecasting the exogenous variables in future in real neuroscience datasets. A key innovation of our approach is to leverage a stochastic linear encoder instead of a deterministic representation. We show that stochasticity greatly improves both robustness and generalization across these tasks.

<sup>1</sup>Lawrence Berkeley National Laboratory <sup>2</sup>University of California, Santa Cruz. Correspondence to: Rui Meng <rmeng@lbl.gov>.

We formalize our problem in terms of data generated from a stationary dynamical system and propose an information-theoretic objective information for CPIC that captures both compression complexity between inputs and representations as well as the predictive information in the representation space. Moreover, instead of directly estimating the objective information, we propose variational bounds and develop a tractable end-to-end training framework. We demonstrate CPIC can recover the latent trajectories of noisy dynamical systems with low signal-to-noise ratios. We conduct experiments on two neuroscience datasets, monkey motor cortex (M1) and rat dorsal hippocampus study (HC), and we show that our extracted latent representations have better forecasting capability for the monkey’s future hand position for M1, and for the rat’s future position for HC. The primary contributions of our paper can be summarized as follows:

- We develop a novel information-theoretic framework, Compressed Predictive Information Coding (CPIC), which extracts useful representation in sequential data. It maximizes the predictive information in the representation space while minimizing the compression complexity.
- Instead of using deterministic representations, we employ a stochastic linear encoder, which contributes to better model robustness and model generalization.
- We propose variational bounds of CPIC’s objective function by taking advantage of variational bounds on mutual information and develop a tractable, end-to-end training procedure.
- We demonstrate that compared with the other unsupervised methods, CPIC recovers more accurate latent dynamics in dynamical system with low signal-to-noise ratio, and extracts more predictive features for downstream tasks in neuroscience data.

## 2. Related Work

Mutual information (MI) plays an important role in estimating the relationship between pairs of variables. It is a reparameterization-invariant measure of dependency:

$$I(X, Y) = \mathbb{E}_{p(x,y)} \left[ \log \frac{p(x|y)}{p(x)} \right] \quad (1)$$

It is widely used in computational neuroscience (Dimitrov et al., 2011), visual representation learning (Chen et al., 2020), natural language processing (Oord et al., 2018) and bioinformatics (Lachmann et al., 2016). In representation learning, the mutual information between inputs and representations is used to quantify the quality of the representation and is also closely related to reconstruction error in

the generative models (Kingma & Welling, 2013; Makhzani et al., 2015).

Information bottleneck (IB) is a method for compressing information while retaining predictive capacity (Tishby et al., 2000). Specifically, IB compresses the variable  $X$  into its compressed representation  $Y$  while preserving as much information as possible related to another variable  $R$ . The trade-off is controlled by the trade-off parameter  $\beta$  and IB is formulated as

$$\min \mathcal{L} : \mathcal{L} \equiv I(X; Y) - \beta I(Y; R). \quad (2)$$

The first term minimizes the complexity of the mapping while the second term increases the capability of the compressed data  $Y$  to predict  $R$ . However, estimating the mutual information in the IB is computationally and statistically challenging except in two cases: discrete data, as in (Tishby et al., 2000) and Gaussian data, as in (Chechik et al., 2005). However, these assumptions both severely constrain the class of learnable models (Alemi et al., 2016). Recent works leverage deep learning models to obtain both differentiable and scalable MI estimation (Belghazi et al., 2018; Nguyen et al., 2010; Oord et al., 2018; Alemi et al., 2016; Poole et al., 2019; Cheng et al., 2020).

In terms of sequential data, (Creutzig & Sprekeler, 2008) utilize the IB method and develops an information-theoretic objective function. (Creutzig et al., 2009) propose another IB objective function based on a specific state-space model. Recently, (Clark et al., 2019) propose Dynamical Components Analysis (DCA), an unsupervised learning approach to extract a subspace with maximal dynamical structure. DCA assumes that data are stationary multivariate Gaussian process and consider a linear mapping to compress data into a low-dimensional subspace and then maximize the predictive information (PI). Due to the gaussian assumption, the mutual information can be expressed in a differentiable closed form with respect to model parameters (Chechik et al., 2005).

All of the above unsupervised representation learning models assume the data to be Gaussian, which may be not realistic, especially when applied to neuroscientific datasets (O’Doherty et al., 2017; Glaser et al., 2020). Therefore, we leverage recently introduced lower bounds on mutual information to construct lower bounds of the CPIC objective and develop end-to-end training procedures.

## 3. Compressed Predictive Information Coding

The main intuition behind Compressed Predictive Information Coding (CPIC) is to extract a robust subspace with minimal compression complexity and maximal dynamical structure. Specifically, CPIC first discards low-level information and noise that is more local by minimizing com-

pression complexity between inputs and representations to help model generalizations. Secondly, CPIC maximizes the predictive information in the representation space. There are different approaches to quantify the predictive capability in the literature: (Wiskott & Sejnowski, 2002; Turner & Sahani, 2007) target on extracting the slowly varying features; (Creutzig & Sprekeler, 2008; Creutzig et al., 2009) maximize the predictive information between past input and future input at single time stamp. Recently, (Clark et al., 2019; Bai et al., 2020) extend the input to a window size of inputs in the estimation of predictive information. Note that the predictive information based methods above are estimated based on the Gaussian assumption. CPIC relieves the Gaussian assumption by construction bounds of mutual information based on deep learning models.

Compared with dynamical component analysis (DCA) (Clark et al., 2019), instead of employing a deterministic linear encoder to compress data, we take advantage of a stochastic linear mapping function. Given inputs, the stochastic representation follows Gaussian distributions, with the means encoded linearly while the variances encoded nonlinearly via any neural network structure. Avoiding the Gaussian assumption on mutual information (Creutzig & Sprekeler, 2008; Creutzig et al., 2009; Clark et al., 2019; Bai et al., 2020), CPIC leverages deep learning based estimations of mutual information. Specifically, we propose differentiable and scalable bounds of CPIC objective via variational inference, which leads to an end-to-end training.

Let  $X = \{x_t\}, x_t \in \mathbb{R}^N$  be a stationary, discrete time series, and let  $X_{\text{past}} = (x_{-T+1}, \dots, x_0)$  and  $X_{\text{future}} = (x_1, \dots, x_T)$  denote consecutive past and future windows of length  $T$ . Similar to the information bottleneck (IB) (Tishby et al., 2000), the CPIC objective contains a trade-off between two factors. The first seeks to minimize the compression complexity and the second to maximize the predictive information in the representation space. Both deterministic and stochastic linear encoders  $p(Y|X)$  are considered. Note that when the encoder is deterministic the compression complexity is depreciated and when the encoder is stochastic the complexity is measured by the mutual information between representations and inputs. As for the predictive capability, it is measured by predictive information in representation space. In the CPIC objective, the trade-off weight  $\beta > 0$  dictates the balance between the compression and predictive information terms:

$$\min \mathcal{L} : \mathcal{L} \equiv \beta I(X_{\text{past}}; Y_{\text{past}}) - I(Y_{\text{past}}; Y_{\text{future}})$$

$Y_{\text{past}}$  and  $Y_{\text{future}}$  are compressed versions of past and future data. Larger  $\beta$  promotes a more compact mapping and thus benefits model generalization, while smaller  $\beta$  would lead to more predictive information in the representation space on training data. This objective function is visualized in

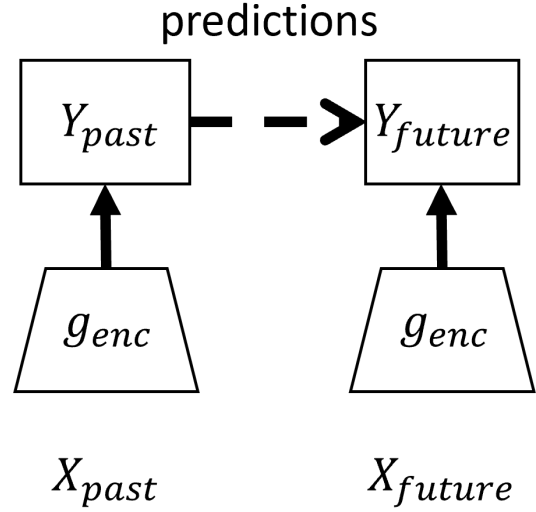


Figure 1. The overall framework of compressed predictive information coding. The encoder compress information of the input  $X$  into  $Y$  such that the predictive information between  $Y_{\text{past}}$  and  $Y_{\text{future}}$  while minimizing the mutual information between  $X$  and  $Y$ .

Figure 1, where inputs  $X$  are encoded into representation space as  $Y$  via tractable encoders and the dynamics of  $Y$  are learned in a model-free manner.

The encoder  $p(Y|X)$  could be implemented by fitting deep neural networks (Alemi et al., 2016) to encode data  $X$ . Instead, CPIC takes an approach similar to VAEs (Kingma & Welling, 2013), in that it encodes data into stochastic representations. Specifically, CPIC uses a simple stochastic linear encoder ( $g_{\text{enc}}$  in Figure 1) to compress input  $x_t$  into  $y_t$  as

$$y_t|x_t \sim \mathcal{N}(\mu_t, \text{diag}(\sigma_t^2)), \quad (3)$$

for each time stamp  $t$ . The mean of  $y_t$  is given by a linear mapping  $\mu_t = U^T x_t$ ,  $U \in \mathbb{R}^{N \times D}$  whereas the variance arises from a nonlinear mapping  $\sigma_t = g^{\text{Encoder}}(x_t)$ . The nonlinear mapping can be modeled by any neural network architecture. For simplicity, we use a two-layer perceptron. Note that when  $\sigma_t = 0$ , this encoder reduces to a deterministic linear encoder.

Given a specified window size  $T$ , the relation between past/future blocks of input data  $X(-T), X(T) \in \mathbb{R}^{N \times T}$  and encoded data  $Y(-T), Y(T) \in \mathbb{R}^{Q \times T}$  are equivalent,  $p(X(-T), Y(-T)) = p(X(T), Y(T))$ , due to the stationary assumption. Without loss of generality, the compression relation can be expressed as

$$Y(T) = U^T X(T) + \xi(T) \quad (4)$$

where  $\xi(T) \in \mathcal{N}(0, \text{blockdiag}(\text{diag}(\sigma_1^2), \dots, \text{diag}(\sigma_T^2)))$  and variance of noise  $\sigma_t^2$  depends on the input  $x_t$ .

### 3.1. Relation to Past-future Information Bottleneck

CPIC is related to the past-future information bottleneck (PFIB) in (Creutzig & Sprekeler, 2008; Creutzig et al., 2009). There are two primary differences. First, PFIB only compresses the past information, while CPIC compresses both the past and the future. The intuition behind this is similar to that in (Oord et al., 2018): we want to discard low-level information and localized noise by maximizing the mutual information between the two in the representation space. By using a linear encoder, CPIC eases interpretation of optimal subspace with minimal compression complexity and maximal dynamical structure. Second, PFIB makes a Gaussian assumption (Chechik et al., 2005) in terms of estimation of mutual information, while CPIC does not make any assumption on the data. Recently, (Wang et al., 2019) utilize the PFIB framework to learn the minimally complex yet most predictive representation. That work has two primary drawbacks. It considers a deterministic linear encoder, directly ignoring the effect of complexity in compression, and it directly utilizes a neural network to build the relation between past and future, which may have a profound effect on the expressiveness of the model.

## 4. Variational Bounds of Compressed Predictive Information Coding

In the CPIC, since data  $X$  are stationary, the mutual information for the past is equivalent to that for the future  $I(X(-T); Y(-T)) = I(X(T); Y(T))$ . Therefore, the objective of CPIC can be rewritten as

$$\min \mathcal{L} = \beta I(X(T); Y(T)) - I(Y(-T); Y(T)). \quad (5)$$

We develop the variational upper bounds on the mutual information for the compression complexity  $I(X(T); Y(T))$  and lower bounds on mutual information for the predictive capacity  $I(Y(-T); Y(T))$ .

### 4.1. Upper Bounds of Compression Complexity

Directly estimating compression complexity  $I(X(T); Y(T)) := \mathbb{E}_{X(T)} [\text{KL}(p(y(T)|x(T)), p(y(T)))]$  is intractable, because the population distribution  $p(y(T))$  is unknown. Thus we introduce a variational approximation to the marginal distribution of encoded inputs  $p(y(T))$ , denoted as  $r(y(T))$ . Due to the non-negativity of the Kullback-Leibler (KL) divergence, we can derive the variational upper bound as

$$\begin{aligned} I(X(T); Y(T)) &= \mathbb{E}_{X(T)} [\text{KL}(p(y(T)|x(T)), r(y(T))) \\ &\quad - \text{KL}(p(y(T)), r(y(T)))] \\ &\leq \mathbb{E}_{X(T)} [\text{KL}(p(y(T)|x(T)), r(y(T)))] \\ &= I_{\text{VUB}}(X(T); Y(T)). \end{aligned} \quad (6)$$

Generally, learning  $r(y(T))$  was recognised as the distribution density estimation problem (Silverman, 2018), which is challenging. In this setting, the variational distribution  $r(y(T))$  is assumed to be learnable, and thus estimating the variational upper bound is tractable. In particular, Alemi et al. (2016) fix  $r(y(T))$  as a standard normal distribution, leading to high-bias in MI estimation. Recently, Poole et al. (2019) replace  $r(y(T))$  with a Monte Carlo approximation. Specifically, with  $S$  sample pairs  $(x(T)_i, y(T)_i)_{i=1}^S$ ,  $r_i(y(T)) = \frac{1}{S-1} \sum_{j \neq i} p(y(T)|x(T)_j) \approx p(y(T))$  and Poole et al. (2019) derive a leave-one-out upper bound (L1Out) as below:

$$\begin{aligned} I_{\text{L1Out}}(X(T); Y(T)) \\ &= \mathbb{E} \left[ \frac{1}{S} \sum_{i=1}^S \left[ \log \frac{p(y(T)_i|x(T)_i)}{\frac{1}{S-1} \sum_{j \neq i} p(y(T)_i|x(T)_j)} \right] \right]. \end{aligned} \quad (7)$$

In practice, L1Out bound depends on the sample size  $S$  and may suffer from numerical instability. Thus, we would like to choose the sample size  $S$  as large as possible. In general scenarios where  $p(y(T)|x(T))$  is intractable, Cheng et al. (2020) propose the variational versions of VUB and L1Out by using a neural network to approximate the condition distribution  $p(y(T)|x(T))$  in (6) and (7). Since CPIC leverages a known stochastic/deterministic linear encoder, VUB and L1Out estimators are considered in the construction of CPIC variational bounds.

### 4.2. Lower Bounds of Predictive Information

As for the predictive information (PI), we would derive lower bounds of  $I(Y(-T); Y(T))$  using results in (Agakov, 2004; Alemi et al., 2016; Poole et al., 2019). First, similar to Agakov (2004), we replace the intractable conditional distribution  $p(y(T)|y(-T))$  with a tractable optimization problem over a variational conditional distribution  $q(y(T)|y(-T))$ . It yields a lower bound on PI due to the non-negativity of the KL divergence:

$$\begin{aligned} I(Y(-T); Y(T)) &\geq H(Y(T)) \\ &\quad + \mathbb{E}_{p(y(-T), y(T))} [\log q(y(T)|y(-T))] \end{aligned} \quad (8)$$

where  $H(Y)$  is the differential entropy of variable  $Y$  and this bound is tight if and only if  $q(y(T)|y(-T)) = p(y(T)|y(-T))$ , suggesting that the second term in (8) equals the negative conditional entropy  $-H(Y(T)|Y(-T))$ .

Because  $H(Y(T)) \geq 0$  has no information about the dependence between  $Y(-T)$  and  $Y(T)$ , it leads to a looser lower bound by ignoring it as the same in (Agakov, 2004) such

that

$$I(Y(-T), Y(T)) \geq \int \mathbb{E}_{p(y(-T), y(T))} [\log q(y(T)|y(-T))] \triangleq I_{\text{LBA}}(Y(-T), Y(T)). \quad (9)$$

The conditional expectation in (9) can be estimated using Monte Carlo sampling based on the encoded data distribution  $p(y(-T), y(T))$ . And encoded data are sampled by introducing the augmented data  $x(-T)$  and  $x(T)$  and marginalizing them out as

$$p(y(-T), y(T)) = \int p(x(-T), x(T)) p(y(-T)|x(-T)) p(y(T)|x(T)) dx(-T)x(T) \quad (10)$$

according to the Markov chain proposed in Figure 1.

However, this lower bound requires a tractable decoder for the conditional distribution  $q(y|x)$  (Alemi et al., 2016). Alternatively, according to (Poole et al., 2019), by considering an energy-based variational family to express and conditional distribution  $q(y(T)|y(-T))$ :

$$q(y(T)|y(-T)) = \frac{p(y(T))e^{f(y(T), y(-T))}}{Z(y(-T))}$$

where  $f(x, y)$  is a differentiable critic function,  $Z(y(-T)) = \mathbb{E}_{p(y(T))} [e^{f(y(T), y(-T))}]$  is a partition function, and introducing a baseline function  $a(y(T))$ , we derive a tractable unnormalized Barber and Agakov (TUBA) lower bound of the predictive information as:

$$I(Y(-T), Y(T)) \geq \mathbb{E}_{p(y(-T), y(T))} [\tilde{f}(y(-T), y(T))] - \log \left( \mathbb{E}_{p(y(-T))p(y(T))} [e^{\tilde{f}(y(-T), y(T))}] \right) \triangleq I_{\text{TUBA}}(Y(-T), Y(T)) \quad (11)$$

where  $\tilde{f}(y(-T), y(T)) = f(y(-T), y(T)) - \log(a(y(T)))$  is treated as an updated critic function. Notice that different choices of baseline functions lead to different mutual information estimators. When  $a(y(T)) = 1$ , it leads to mutual information neural estimator (MINE) (Belghazi et al., 2018); when  $a(y(T)) = Z(y(T))$ , it leads to the lower bound proposed in (Donsker & Varadhan, 1975) (DV) and when  $a(y(T)) = e$ , it recovers the lower bound in (Nguyen et al., 2010) (NWJ) also known as f-GAN (Nowozin et al., 2016) and MINE-f (Belghazi et al., 2018). In general, the critic function  $f(x, y)$  and the log baseline function  $a(y)$  are usually parameterized by neural networks (Oord et al., 2018; Belghazi et al., 2018). Especially, Oord et al. (2018) use a separable critic function  $f(x, y) = h_\theta(x)^T g_\theta(y)$  while Belghazi et al. (2018) use a joint critic function  $f(x, y) = f_\theta(x, y)$ . (Poole et al., 2019) claim that joint critic function generally performs better than separable critic function but scale poorly with batch size.

However, all MI estimators in the form of (11) have high variance due to the high variance of  $f(x, y)$ . Oord et al. (2018) propose a low-variance MI estimator based on noise-contrastive estimation called InfoNCE. In our case, the lower bound of predictive information is derived as

$$I(Y(-T); Y(T)) \geq \mathbb{E} \left[ \frac{1}{S} \sum_{i=1}^S \log \frac{e^{f(y(-T)_i, y(T)_i)}}{\frac{1}{S} \sum_{j=1}^S e^{f(y(-T)_i, y(T)_j)}} \right] \quad (12)$$

The expectation is over  $S$  independent samples from the joint distribution:  $p(y(-T), y(T))$  with the same sampling procedure in (10).

### 4.3. Variational Bounds of CPIC

We propose two classes of lower bounds of CPIC based on whether the bounds depend on multiple samples. We name the first class as Uni-sample lower bounds, which take the VUB upper bound of mutual information for the complexity of data compression  $I(X(T), Y(T))$  and the TUBA as the lower bound of predictive information in (11). Thus we have

$$\mathcal{L}_{\text{UNI}} = \beta \text{KL}(p(y(T)|x(T)), r(y(T))) - I_{\text{TUBA}}(Y(-T), Y(T)). \quad (13)$$

Notice that by choosing different baseline functions, the lower bounds are equivalent to different mutual information estimators such as MINE, DV and NWJ. The second class is named as multiple-sample lower bounds, which take advantage of the noise-contrastive estimation trick. And the multi-sample lower bounds are expressed as

$$\mathcal{L}_{\text{MUL}} = \beta \mathbb{E} \left[ \frac{1}{S} \sum_{i=1}^S \left[ \log \frac{p(y(T)_i|x(T)_i)}{\frac{1}{S-1} \sum_{j \neq i} p(y(T)_i|x(T)_j)} \right] \right] - \mathbb{E} \left[ \frac{1}{S} \sum_{i=1}^S \log \frac{e^{f(y(-T)_i, y(T)_i)}}{\frac{1}{S} \sum_{j=1}^S e^{f(y(-T)_i, y(T)_j)}} \right]. \quad (14)$$

Two main differences exist between these two classes of lower bounds. First, the performance of multiple-sample lower bounds depend on batch size while uni-sample lower bounds do not. Secondly, multiple-sample lower bounds have lower variance than uni-sample lower bounds. Without any specification, we assume that CPIC employs the multiple-sample lower bound.

On the other hand, we classify the lower bounds into stochastic and deterministic version by whether we employ a deterministic or stochastic encoder. Notice that when choosing the deterministic encoder, the compression complexity term (first term) in (13) and (14) are constant.

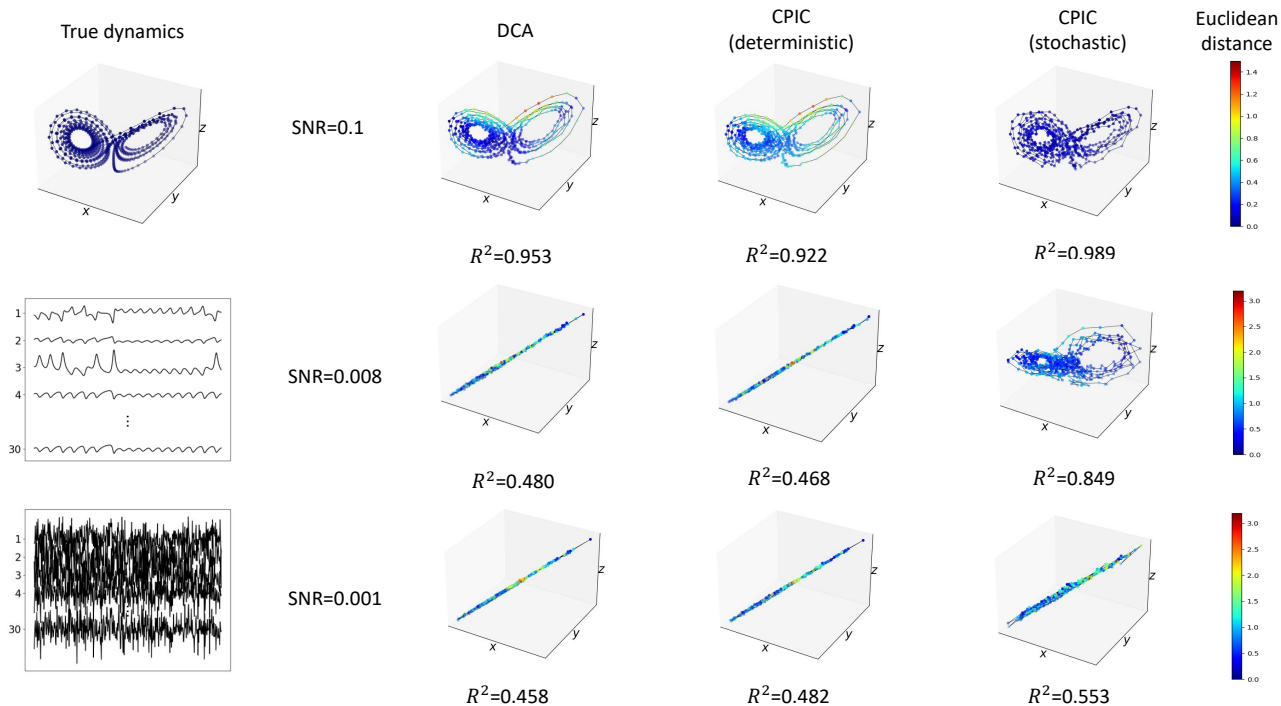


**Figure 2. Left panel.** Top: 3D trajectories of Lorenz attractor’s ground-truth. Middle: 30D projected trajectory. Bottom: Corrupted 30D trajectory with SNR=0.001. **Right Panel.** 3D trajectories obtained by DCA, deterministic CPIC, and stochastic CPIC methods with respect to different SNRs (0.1, 0.008, 0.001). We encode the point-wise Euclidean distance between the aligned inferred latent dynamics and the true dynamics into color on trajectories. Color from blue to red corresponds to the distance from short to long respectively. Separate colorbars are used for their corresponding SNRs. Stochastic CPIC outperforms DCA and deterministic CPIC with more similar dynamics pattern and smaller point-wise errors.

## 5. Experiments

In this section, we illustrate the performance of CPIC in both synthetic and real data experiments. We first show the reconstruction performance of CPIC in noisy dynamical system on one tractable experiment (noisy Lorenz attractor). We demonstrate that CPIC recovers more accurate latent dynamics compared with other unsupervised methods. Secondly, for further demonstrating the benefits of the latent representations, we conduct forecasting of exogenous variables using simple linear models from neuroscience data sets. The motivation for using linear forecasting models is that good representations contribute to disentangling complex data in a linearly accessible way. Specifically, we extract latent representations and then conduct forecasting tasks given the inferred representations on two neuroscience datasets: multi-neuronal recordings from the hippocampus (HC) while rats navigate a maze (Glaser et al., 2020) and multi-neuronal recordings from primary motor cortex (M1) during a reaching task for monkeys (O’Doherty et al., 2017). The experimental results show that CPIC has better predictive performance on those forecasting tasks comparing with

existing methods.

### 5.1. Noisy Lorenz Attractor

The Lorenz attractor is a 3D time series that are realizations of the Lorenz dynamical system (Pchelintsev, 2014). It describes a two dimensional flow of fluids with latent processes given as:

$$\begin{aligned} \frac{df_1}{dt} &= \sigma(f_2 - f_1), \frac{df_2}{dt} = f_1(\rho - f_3) - f_2, \\ \frac{df_3}{dt} &= f_1 y - \beta f_3. \end{aligned} \quad (15)$$

Lorenz sets the values  $\sigma = 10$ ,  $\beta = 8/3$  and  $\rho = 28$  to exhibit a chaotic behavior, as done in recent works (She & Wu, 2020; Clark et al., 2019; Zhao & Park, 2017; Linderman et al., 2017). We simulate the latent signals from the Lorenz dynamical system and show them in the left-top panel in Figure 2. Then we map the 3D latent signals to 30D lifted observations with a random linear embedding in the left-middle panel and add spatially anisotropic Gaussian noise on the 30D lifted observations in the left-bottom panel. The

noises are generated according to different signal-to-noise ratios (SNRs), where SNR is defined by the ratio of the variance of the first principle components of dynamics and noise as in (Clark et al., 2019). Specifically, we propose 10 different SNR levels spaced evenly on a log (base 10) scale between  $[-3, -1]$  and corrupt the 30D lifted observations with noise corresponding to different SNR levels. Finally, we deploy different representation learning methods to recover the true 3D dynamics from different corrupted 30D lifted observations with different SNR levels, and compare the accuracy of recovering the underlying Lorenz attractor time-series.

We first compare stochastic CPIC with deterministic CPIC and the DCA method. For both CPIC methods, we take multiple-sample lower bounds  $\mathcal{L}_{\text{MUL}}$ . We set the latent dimension size  $Q = 3$  and the time window size  $T = 4$ . We aligned the inferred latent trajectory with the true 3D dynamics with optimal linear mapping due to the reparameterization-invariant measure of latent trajectories. We validate the reconstruction performance based on the  $R^2$  regression score. For all three methods, aligned latent trajectories inferred from corrupted lifted observation with different SNR = 0.001, 0.008 and 0.1 levels of noise as well as  $R^2$  scores are shown in Figure 2. The point-wise distances between the recovered dynamics and the ground-truth dynamics are encoded into different colors from blue to red, representing the distance from short to long. For high SNR (SNR = 0.1, top-right), all methods did a good job of recovering the Lorenz dynamics and the stochastic CPIC had larger  $R^2$  than both DCA and CPIC. For intermediate SNR (SNR = 0.008, middle-right), we see that DCA and deterministic CPIC completely fail at recovering the ground truth dynamics, while stochastic CPIC performs reasonably. Finally, as the SNR gets lower (SNR = 0.001, bottom-right) all methods perform poorly, but stochastic CPIC has higher  $R^2$  scores than others. These results suggest that stochastic CPIC outperforms its deterministic version and DCA across different SNRs.

To better illustrate the latent dynamics recovery in terms of different SNRs, we plot the  $R^2$  scores from stochastic CPIC and DCA method for all ten SNR levels with uncertainty quantification in Figure 3. The uncertainty quantification is visualized by one standard deviation below and above and mean of ten  $R^2$  scores with respect to their corresponding ten random initializations. As suggested by the examples in Figure 2, it shows that stochastic CPIC robustly outperforms DCA in recovering latent dynamics, and in particular, the SNR at which reasonable recovery is lower for stochastic CPIC than DCA. In addition, we conducted another experiment to compare the performance of uni-sample lower bounds and multi-sample lower bounds between the deterministic and stochastic versions of CPIC. The CPIC with uni-sample lower bounds refers to those with NWJ, MINE,

and TUBA estimates of predictive information (P). The CPIC with multiple-sample lower bound refers to that with NEC estimate of PI. We report the performance among these four variants of objectives in both deterministic and stochastic CPICs in appendix (Table 2). We find that stochastic CPIC with multiple-sample lower bounds has better reconstruction performance of latent dynamics in majority levels of noisy data.

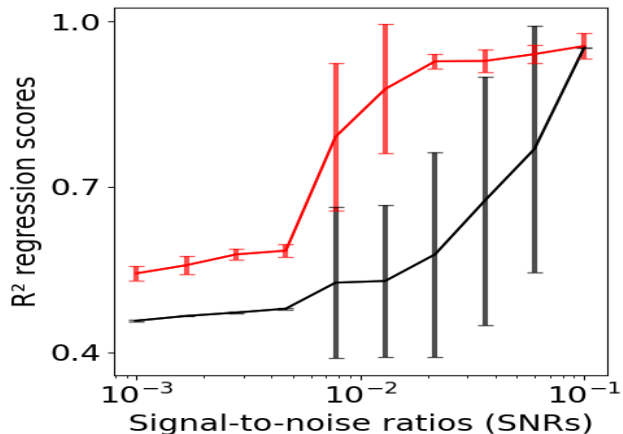


Figure 3. Comparison on  $R^2$  scores of latent dynamics regression between DCA and stochastic CPIC with the mean and one standard deviation above/below it over running ten different random initializations.

## 5.2. Forecasting Exogenous Variables from Multi-neuronal Recordings with Linear Decoding

In this section, we show that latent representations extracted by stochastic CPIC perform better in the downstream forecasting tasks on two neuroscience datasets: multi-neuron recordings from monkey motor cortex (M1) during a reaching task (O’Doherty et al., 2017) and multi-neuron recordings from rat dorsal hippocampus (HC) during maze navigation (Glaser et al., 2020). We compared stochastic CPIC with PCA and DCA. For each model, we extract the latent representations and conduct prediction tasks on the relevant exogenous variable at a future time step. For example, for the M1 dataset, we extract a consecutive 3-length window representation of multi-neuronal spiking activity to predict the monkey’s arm position in a future time step which is *lag* time stamps away. The predictions are conducted by linear regression<sup>1</sup> to emphasize the structure learned by the unsupervised methods. For these tasks,  $R^2$  regression score is used as the evaluation metric to measure the forecasting performance.  $R^2$  regression scores were calculated using 5-fold cross validation. We considered three different lag values (5, 10, and 15), and considered four different window

<sup>1</sup>[https://scikit-learn.org/stable/modules/linear\\_model.html](https://scikit-learn.org/stable/modules/linear_model.html)

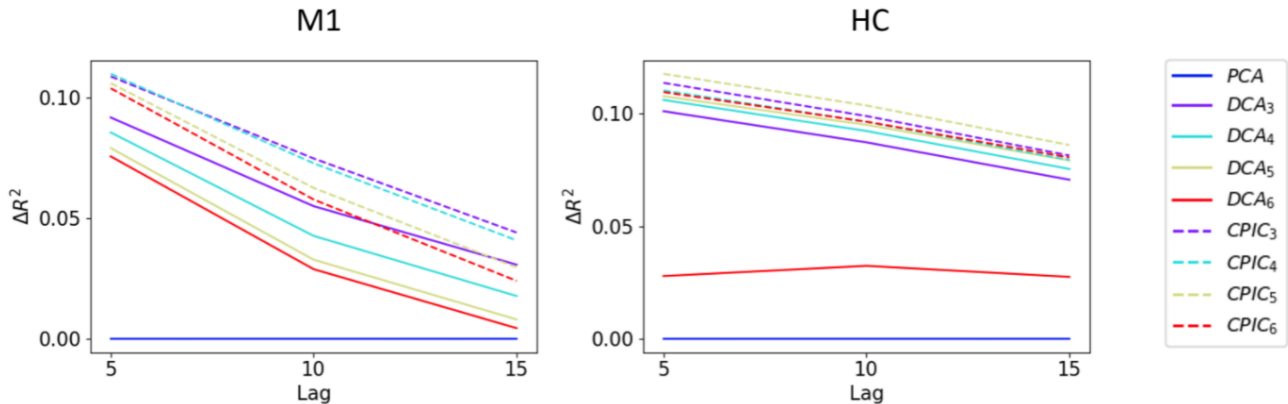


Figure 4. Comparison between different methods (PCA, DCA, and stochastic CPIC) on  $R^2$  regression scores for two forecasting tasks with three different lag values (5, 10, and 15).  $R^2$  values are averaged across five folds. For DCA and stochastic CPIC models using predictive information loss, we test them with four time window sizes ( $T = 3, 4, 5, 6$ ). The subscript refers to the window size of past and future time series. Left: motor cortex (M1). Right: dorsal hippocampus (HC).

Dataset	Lag	DCA	CPIC			
			Deterministic	Improvement over DCA	Stochastic	Improvement over DCA
M1	5	0.251	0.265	5.58%	0.268	6.77%
	10	0.259	0.275	6.18%	0.279	7.72%
	15	0.210	0.222	5.71%	0.224	6.67%
HC	5	0.149	0.147	-1.34%	0.159	6.71%
	10	0.132	0.131	0.76%	0.141	6.82%
	15	0.111	0.110	-0.90%	0.118	6.31%

Table 1. Comparison between DCA, deterministic CPIC and stochastic CPIC on  $R^2$  regression scores on M1 and HC datasets with the optimal window size among  $T \in [3, 4, 5, 6]$  for three different lag values (5, 10, and 15).  $R^2$  regression scores are averaged across five folds. We report the deterministic CPIC’s and stochastic CPIC’s improvement (percentage) over DCA and it shows that stochastic CPIC robustly improves the forecasting performance on downstream tasks.

sizes  $T = 3, 4, 5, 6$  in both DCA and stochastic CPIC.

The results of this analysis are visualized in Figure 4. Generally, a larger *lag* value leads to a more challenging forecasting task. Importantly, we observe that models utilizing the predictive information loss perform much better than PCA, and moreover, stochastic CPIC leads to consistently better prediction performance than DCA on any fixed window size  $T$  for all forecasting tasks. This demonstrates that stochastic CPIC extracts more useful information than DCA in these complex neuroscience datasets. Moreover, we also find that different settings of window size impact the  $R^2$  regression score. M1 obtains the best  $R^2$  when the window size is set to 3. For HC, it is 5. Similar to DCA, the optimal window size of past/future data depends on the characteristics of datasets as well as the specified downstream tasks. Finally, we show the necessity of the stochastic encoder by comparing deterministic CPIC with stochastic CPIC on M1 and HC datasets on all lag values. We choose the optimal window size  $T \in [3, 4, 5, 6]$  for stochastic CPIC, which

is  $T = 3$  for M1 and  $T = 5$  for HC. The  $R^2$  scores for DCA, deterministic CPIC and stochastic CPIC are shown in Table 1 on their improvement over DCA. Together, these results suggest that stochastic CPIC robustly improves the predictive performance on downstream tasks comparing to DCA and deterministic CPIC.

## 6. Concluding Remarks

We developed a novel information-theoretic framework, Compressed Predictive Information Coding, to extract useful representations in sequential data. CPIC maximizes the predictive information in representation space while minimizing the compression complexity. We leverage stochastic representations by employing a stochastic linear encoder and propose variational bounds of the CPIC objective function. We demonstrate that CPIC can extract more accurate low-dimensional latent dynamics and more useful representations that has better forecasting performance of downstream tasks on two neuroscience datasets. Together, these



results suggest that CPIC will yield similar improvements in other datasets.

## References

- Agakov, D. B. F. The im algorithm: a variational approach to information maximization. *Advances in neural information processing systems*, 16(320):201, 2004.
- Alemi, A. A., Fischer, I., Dillon, J. V., and Murphy, K. Deep variational information bottleneck. *arXiv preprint arXiv:1612.00410*, 2016.
- Baevski, A., Zhou, H., Mohamed, A., and Auli, M. wav2vec 2.0: A framework for self-supervised learning of speech representations. *arXiv preprint arXiv:2006.11477*, 2020.
- Bai, J., Wang, W., Zhou, Y., and Xiong, C. Representation learning for sequence data with deep autoencoding predictive components. *arXiv preprint arXiv:2010.03135*, 2020.
- Belghazi, M. I., Baratin, A., Rajeswar, S., Ozair, S., Bengio, Y., Courville, A., and Hjelm, R. D. Mine: mutual information neural estimation. *arXiv preprint arXiv:1801.04062*, 2018.
- Bengio, Y., Courville, A., and Vincent, P. Representation learning: A review and new perspectives. *IEEE transactions on pattern analysis and machine intelligence*, 35(8):1798–1828, 2013.
- Bialek, W., Nemenman, I., and Tishby, N. Predictability, complexity, and learning. *Neural computation*, 13(11):2409–2463, 2001.
- Brown, T. B., Mann, B., Ryder, N., Subbiah, M., Kaplan, J., Dhariwal, P., Neelakantan, A., Shyam, P., Sastry, G., Askell, A., et al. Language models are few-shot learners. *arXiv preprint arXiv:2005.14165*, 2020.
- Chechik, G., Globerson, A., Tishby, N., Weiss, Y., and Dayan, P. Information bottleneck for gaussian variables. *Journal of machine learning research*, 6(1), 2005.
- Chen, T., Kornblith, S., Norouzi, M., and Hinton, G. A simple framework for contrastive learning of visual representations. In *International conference on machine learning*, pp. 1597–1607. PMLR, 2020.
- Cheng, P., Hao, W., Dai, S., Liu, J., Gan, Z., and Carin, L. Club: A contrastive log-ratio upper bound of mutual information. In *International Conference on Machine Learning*, pp. 1779–1788. PMLR, 2020.
- Clark, D. G., Livezey, J. A., and Bouchard, K. E. Unsupervised discovery of temporal structure in noisy data with dynamical components analysis. *arXiv preprint arXiv:1905.09944*, 2019.
- Creutzig, F. and Sprekeler, H. Predictive coding and the slowness principle: An information-theoretic approach. *Neural Computation*, 20(4):1026–1041, 2008.
- Creutzig, F., Globerson, A., and Tishby, N. Past-future information bottleneck in dynamical systems. *Physical Review E*, 79(4):041925, 2009.
- Devlin, J., Chang, M.-W., Lee, K., and Toutanova, K. Bert: Pre-training of deep bidirectional transformers for language understanding. *arXiv preprint arXiv:1810.04805*, 2018.
- Dimitrov, A. G., Lazar, A. A., and Victor, J. D. Information theory in neuroscience. *Journal of computational neuroscience*, 30(1):1–5, 2011.
- Donsker, M. D. and Varadhan, S. S. Asymptotic evaluation of certain markov process expectations for large time, i. *Communications on Pure and Applied Mathematics*, 28(1):1–47, 1975.
- Glaser, J. I., Benjamin, A. S., Chowdhury, R. H., Perich, M. G., Miller, L. E., and Kording, K. P. Machine learning for neural decoding. *Eneuro*, 7(4), 2020.
- Goodfellow, I., Pouget-Abadie, J., Mirza, M., Xu, B., Warde-Farley, D., Ozair, S., Courville, A., and Bengio, Y. Generative adversarial nets. *Advances in neural information processing systems*, 27, 2014.
- Grill, J.-B., Strub, F., Altché, F., Tallec, C., Richemond, P. H., Buchatskaya, E., Doersch, C., Pires, B. A., Guo, Z. D., Azar, M. G., et al. Bootstrap your own latent: A new approach to self-supervised learning. *arXiv preprint arXiv:2006.07733*, 2020.
- He, K., Fan, H., Wu, Y., Xie, S., and Girshick, R. Momentum contrast for unsupervised visual representation learning. In *Proceedings of the IEEE/CVF Conference on Computer Vision and Pattern Recognition*, pp. 9729–9738, 2020.
- Kingma, D. P. and Welling, M. Auto-encoding variational bayes. *arXiv preprint arXiv:1312.6114*, 2013.
- Lachmann, A., Giorgi, F. M., Lopez, G., and Califano, A. Aracne-ap: gene network reverse engineering through adaptive partitioning inference of mutual information. *Bioinformatics*, 32(14):2233–2235, 2016.
- Linderman, S., Johnson, M., Miller, A., Adams, R., Blei, D., and Paninski, L. Bayesian learning and inference in recurrent switching linear dynamical systems. In *Artificial Intelligence and Statistics*, pp. 914–922. PMLR, 2017.
- Makhzani, A., Shlens, J., Jaitly, N., Goodfellow, I., and Frey, B. Adversarial autoencoders. *arXiv preprint arXiv:1511.05644*, 2015.
- Nguyen, X., Wainwright, M. J., and Jordan, M. I. Estimating divergence functionals and the likelihood ratio by convex

- risk minimization. *IEEE Transactions on Information Theory*, 56(11):5847–5861, 2010.
- Nowozin, S., Cseke, B., and Tomioka, R. f-gan: Training generative neural samplers using variational divergence minimization. In *Proceedings of the 30th International Conference on Neural Information Processing Systems*, pp. 271–279, 2016.
- Oord, A. v. d., Li, Y., and Vinyals, O. Representation learning with contrastive predictive coding. *arXiv preprint arXiv:1807.03748*, 2018.
- O’Doherty, J. E., Cardoso, M., Makin, J., and Sabes, P. Nonhuman primate reaching with multichannel sensorimotor cortex electrophysiology. *Zenodo* <http://doi.org/10.5281/zenodo.583331>, 2017.
- Pchelintsev, A. Numerical and physical modeling of the dynamics of the lorenz system. *Numerical analysis and Applications*, 7(2):159–167, 2014.
- Poole, B., Ozair, S., Van Den Oord, A., Alemi, A., and Tucker, G. On variational bounds of mutual information. In *International Conference on Machine Learning*, pp. 5171–5180. PMLR, 2019.
- She, Q. and Wu, A. Neural dynamics discovery via gaussian process recurrent neural networks. In *Uncertainty in Artificial Intelligence*, pp. 454–464. PMLR, 2020.
- Silverman, B. W. *Density estimation for statistics and data analysis*. Routledge, 2018.
- Tishby, N., Pereira, F. C., and Bialek, W. The information bottleneck method. *arXiv preprint physics/0004057*, 2000.
- Turner, R. and Sahani, M. A maximum-likelihood interpretation for slow feature analysis. *Neural computation*, 19(4):1022–1038, 2007.
- Wang, W., Tang, Q., and Livescu, K. Unsupervised pre-training of bidirectional speech encoders via masked reconstruction. In *ICASSP 2020-2020 IEEE International Conference on Acoustics, Speech and Signal Processing (ICASSP)*, pp. 6889–6893. IEEE, 2020.
- Wang, Y., Ribeiro, J. M. L., and Tiwary, P. Past–future information bottleneck for sampling molecular reaction coordinate simultaneously with thermodynamics and kinetics. *Nature communications*, 10(1):1–8, 2019.
- Wiskott, L. and Sejnowski, T. J. Slow feature analysis: Unsupervised learning of invariances. *Neural computation*, 14(4):715–770, 2002.
- Zhao, Y. and Park, I. M. Variational latent gaussian process for recovering single-trial dynamics from population spike trains. *Neural computation*, 29(5):1293–1316, 2017.

### A. Comparison between DCA, deterministic & stochastic CIPC (four different variational lower bounds) on $R^2$ regression score

In this section, the  $R^2$  regression scores for DCA, deterministic & stochastic CIPC (NWJ, MINE, TUBA, and NEC lower bounds) for all ten different SNRs are reported in Table 2. Generally, It shows that stochastic CIPC with multiple-sample lower bound outperforms other approaches in majority of SNRs.

Signal Noise Ratio	DCA	CIPC							
		deterministic				stochastic			
		NWJ	MINE	TUBA	NEC	NWJ	MINE	TUBA	NEC
SNR = 0.001	0.458	<b>0.554</b>	0.543	0.547	0.482	0.539	0.550	0.553	0.459
SNR = 0.00167	0.466	0.539	0.538	0.574	0.430	0.573	0.569	0.571	<b>0.576</b>
SNR = 0.00278	0.473	0.573	0.573	0.573	0.413	0.587	0.583	<b>0.590</b>	0.588
SNR = 0.00464	0.478	0.579	0.562	0.584	0.438	<b>0.598</b>	0.583	0.556	0.593
SNR = 0.00774	0.480	0.597	0.559	0.515	<b>0.912</b>	0.582	0.579	0.589	0.598
SNR = 0.01292	0.484	0.587	0.596	0.597	0.468	0.580	0.563	0.592	<b>0.923</b>
SNR = 0.02154	0.486	0.590	0.596	0.592	0.688	0.568	0.599	0.864	<b>0.930</b>
SNR = 0.03594	0.491	0.587	0.912	0.594	0.923	0.937	0.632	0.907	<b>0.951</b>
SNR = 0.05995	0.952	0.933	0.837	0.936	0.474	0.970	0.939	0.896	<b>0.970</b>
SNR = 0.1	0.953	0.920	0.893	0.889	0.922	0.926	0.910	0.854	<b>0.989</b>

Table 2.  $R^2$  regression scores for DCA, deterministic & stochastic CIPC (NWJ, MINE, TUBA, and NEC lower bounds) for all ten different SNRs